Title

Ultrashort Time-to-Echo Magnetic Resonance Imaging at 3 T for the Detection of Spondylolysis in Cadaveric Spines

Journal

Investigative Radiology, 54(1)

ISSN

0020-9996

Authors

Finkenstaedt, Tim
Siriwanarangsun, Palanan
Achar, Suraj
et al.

Publication Date

2019

DOI

10.1097/rli.0000000000000506

Peer reviewed

HHS Public Access

Author manuscript

Invest Radiol. Author manuscript; available in PMC 2020 January 01.

Published in final edited form as:

Invest Radiol. 2019 January ; 54(1): 32–38. doi:10.1097/RLI.0000000000000506.

Ultrashort Time-to-Echo (UTE) 3-Tesla MRI for the Detection of Spondylolysis in Human Cadavers: Comparison with CT

Tim Finkenstaedt, MD[1,2], **Palanan Siriwananrangsun, MD**[1,3], **Suraj Achar, MD**[4], **Michael Carl, PhD**[5], **Sina Finkenstaedt, MD**[6], **Nirusha Abeydeera, BS**[1,7], **Christine B. Chung, MD**[1,7] **[Prof.]**, and **Won C. Bae, PhD**[1,7]

[1.]Department of Radiology, University of California, San Diego, La Jolla, CA [2.]Institute of Diagnostic and Interventional Radiology, University of Zurich, Switzerland [3.]Department of Radiology, Siriraj Hospital, Bangkok, Thailand [4.]Department of Family Medicine, University of California, San Diego, La Jolla, CA [5.]General Electric Healthcare, San Diego, CA [6.]Department of Neurosurgery, University of Zurich, Switzerland [7.]Department of Radiology, VA San Diego Healthcare System, San Diego, CA

Abstract

Objectives: The objective of this study was to compare the diagnostic performance and confidence of conventional, optimized, and ultrashort time-to-echo (UTE) MR protocols for detection of simulated lumbar spondylolysis in human cadavers. Additionally, we sought to demonstrate the feasibility of the UTE technique in subjects with and without spondylolysis.

Materials and Methods: Four human lumbar spine specimens with 46 individual pars interarticularis were randomly left intact (n=26) or received experimental osteotomy (n=20) using a microsurgical saw to simulate spondylolysis. The specimens were imaged using a CT scan along with three “Tiers” of MR protocols at 3-Tesla: Tier 1) conventional lumbar MR protocol; Tier 2) optimized conventional protocol consisting of a sagittal oblique spoiled gradient recall echo and axial oblique T1 and short tau inversion recovery sequences; Tier 3) a sagittal UTE MR sequence. Two blinded readers evaluated the images using a 4-point scale (1=spondylolysis certainly absent, 2=probably absent, 3=probably present, 4= certainly present) at each individual pars. For each imaging protocol, diagnostic performance (sensitivity, specificity, and receiver operating characteristic area under the curve or ROC AUC, using the surgical osteotomy as the reference), and confidence were assessed, and compared using McNemar test. Furthermore, two human subjects were imaged with the conventional and UTE MR protocols to demonstrate feasibility in vivo.

Results: Diagnostic performance was moderate for Tier 1 and 2, with a moderate sensitivity (0.70 to 0.75) and high (1.00) specificity. In contrast, CT and Tier 3 UTE MRI had both high sensitivity (1.00) and specificity (1.00). The sensitivities of CT or Tier 3 were statistically greater than Tier 1 sensitivity (p=0.041) and neared statistical significance when compared to Tier 2 sensitivity (p=0.074). ROC AUC was also significantly greater for CT and Tier 3 (each area=1.00),

Corresponding author: Won C. Bae, Ph.D., Department of Radiology, University of California, San Diego, 9427 Health Sciences Drive, San Diego, CA 92093-0997, TEL: (858) 246-2240, FAX: (866) 387-1895, wbae@ucsd.edu.

compared to the areas for Tier 1 (0.89, p=0.037) or Tier 2 (0.873, p=0.024). Diagnostic confidences of CT or Tier 3 were much greater than other Tiers: Both Tiers 1 and 2 had a large percentage of uncertain (>60 %, p<0.001) or wrong interpretations (>10%, p<0.001), unlike CT or Tier 3 (0% uncertain or wrong interpretations). Preliminary in vivo UTE images clearly depicted intact and fractured pars.

Conclusions: Our study demonstrated that the detection of pars fractures using a single sagittal UTE MR sequence is superior in performance and confidence to conventional and optimized MR protocols at 3-T, while matching those from CT evaluation. Furthermore, we demonstrated the feasibility of in vivo application of the UTE sequence in subjects with and without spondylolysis.

Keywords

spondylolysis; pars interarticularis; pars defect; CT; MRI; Ultrashort Time to Echo; UTE; detection; diagnostic performance; diagnostic confidence

INTRODUCTION

Spondylolysis is defined as a bony defect in the pars interarticularis of the vertebral arch and occurs most commonly at the L5 vertebral level (85–95%) (1, 2). The prevalence of spondylolysis in adults is about 5%, whereas as many as 50% of adolescent athletes with persistent back pain were found to have spondylolysis (3). The pathogenesis is likely related to shear forces from repetitive hyperextension and trunk rotation during the adolescent growth spurt (4, 5). Consequently, the young population is predominately affected. For this reason, exposure to ionizing radiation is a major concern, as they are susceptible to mutagenic radiation and accumulation of radiation exposure throughout the entire life span (6).

In clinical routine, four-view radiographs including bilateral oblique projections (7), or more frequently, computed tomography (CT) examinations (8) are often performed in addition to lumbar spine MRI when a spondylolysis is suspected. Even four-view radiographs feature a low sensitivity of only 59% and produce a radiation effective dose of 1.26 mSv (7). CT is considered as the reference standard for detection of pars fractures and has a calculated effective dose of 6 mSv (9). In recent studies where CT was used as the reference standard, the sensitivity of conventional sagittal and axial MRI for diagnosis of spondylolysis was 73–92% for a variety of acute and chronic pars fractures (10–13). Furthermore, the following conditions are known to hamper the detection of pars defects on MRI: sclerosis of the neck of the pars, partial facetectomy, and especially in older patients, facet joint osteoarthritis as well as hypertrophic new bone formation (10, 14).

To improve MR detection of spondylolysis, optimized MR protocols have been suggested (15, 16). These optimized MRI protocols include axial oblique T1-weighted as well as fat-suppressed fluid-sensitive sequences and reformatted sagittal oblique sequences using a sagittal 3D spoiled gradient echo sequence dataset (15). This improvement to detect spondylolysis is mainly based on the altered alignment of the imaging planes to better match the complex anatomical orientation of the pars which is oriented obliquely to all three

orthogonal planes, as well as fat-suppressed fluid-sensitive sequences that occasionally reveal sufficient signal from the scar tissue filling the pars defect (16).

The reason for somewhat lower sensitivity of these MR protocols to pars fractures is due to short T2 properties of the cortical bone of the pars, and osteofibrous scar tissue within and near the pars defect, whose signals decay rapidly (17, 18) in conventional spin echo MR sequences using echo times (TE) greater than 10 ms. This results in very low contrast between the cortical bone and the pars defect, and an overall hypointense appearance masking the defect. Novel MR techniques, collectively referred to as ultrashort time to echo (UTE) sequences, have overcome this issue using TE of 1 ms or less (19, 20) and acquiring sufficient MR signal from the scar tissue to detect spondylolysis.

We hypothesize that UTE technique is capable of detecting pars fractures as accurately as CT. The objective of this study was to compare the diagnostic performance and confidence of conventional, optimized, and UTE MR protocols for detection of simulated lumbar spondylolysis in human cadavers. Additionally, we sought to demonstrate the feasibility of the UTE technique in subjects with and without spondylolysis.

MATERIALS AND METHODS

The cadaveric study part was exempted from Institutional Review Board (IRB) approval. The in vivo study part was IRB-approved (IRB registration number *blinded for review*). All procedures performed in this study involving human participants were compliant with the regulations of the Health Insurance Portability and Accountability Act (HIPAA). The human participants gave written informed consent for study participation, collection of data, and use of prototype pulse sequences.

Study population

Cadaveric specimens: Four randomly selected human cadaveric lumbar spines obtained as a block of tissue provided by the (*blinded for review*) Anatomical Material Program was used for our study. Twenty-three vertebral segments (vertebra T12-L5 in most cases) equaling 46 individual pars interarticularis from four different cadaveric spines (n=4 donors; three women, one man; mean age: 54 ± 18 years) were available. The spine specimens included the paraspinal muscles and soft tissue structures, and did not have a history of back surgery.

Human Subjects: One 45-year-old male subject (height: 196 cm and weight: 102 kg) and one 46-year-old male subject (height: 170 cm and weight: 61 kg) with chronic lower back pain were retrospectively included in the ancillary in vivo part of our study. These patients were part of a broader imaging study on lower back pain, referred by a sports medicine physician (*initials blinded for review*). No reference standard (e.g., CT) was available for the UTE sequence (i.e., index test) of these patients.

Experimental pars fractures

From the 46 available pars interarticularis, 20 were selected randomly using a computer random number generator, to be fractured experimentally. Remaining 26 pars were left intact. Cadaveric spines were thawed and consecutively operated using a standard midline

posterior approach by a board-certified neurosurgery fellow with expertise in spine surgery (*initials - blinded for review*) with seven years of experience. During the procedure each pars interarticularis was exposed by gentle surgical preparation creating a continuous soft tissue flap on each side to ensure adequate adaptation of the paraspinal soft tissue structures. Visual evaluation of each pars interarticularis ensured that no preexisting structural defect of the pars was present. Experimental fractures were created (n=20 pars), using a surgical oscillating saw (Stryker System 6, Stryker Corp., Kalamazoo, Michigan) with a 0.9–1.0 mm thick microsurgical bone blade (SO6–115 and SO6–131) similar to the technique published by Kepler et al. (21). Our experimental pars fractures would fall between stage II "early spondylolysis" characterized by a hairline fracture and stage III "progressive spondylolysis" characterized by a wide pars defect, according to the spondylolysis classification by Ralston et al. (22). Photo documentation was done after the fractures were performed. Each fracture gap was filled with ~1 ml of 8% agarose solution applied with a syringe with an 18 Gauge needle. After cooling and solidification of the agarose gel the soft tissue structures were meticulously reattached using a deep and superficial suture technique. Subsequently, to prevent air accumulation in the adjacent soft tissue structures each specimen was tightly wrapped in transparent film and vacuum-sealed. The surgical osteotomies served as the reference standard of the presence of pars fracture.

To ensure filling of the experimental fracture gaps with a material featuring similar MR signal characteristics as scar tissue, we tested 30 different materials including agarose (A9539, Sigma-Aldrich, Carlsbad, CA) in different concentrations. The candidate materials were filled in small vials and embedded in a slab of bovine muscle as a surrogate for paraspinal muscle. Out of the candidates, 8% (by weight) agarose gel was selected as most suitable.

MR Imaging

All MRI was performed on a 3-T GE MR Discovery 750 scanner (GE Healthcare, Milwaukee, WI) with a standard spine array coil on the following day after the experimental fractures were surgically induced. Three "Tiers" of MR protocols for the lumbar spine were created: 1) conventional, 2) optimized conventional, and 3) novel UTE MR sequences.

Tier 1, conventional MR protocol constituted of a standard lumbar MR protocol (Table 1). Tier 2, optimized conventional MR protocol constituted of conventional MR sequences using imaging planes that are optimally aligned to the plane of the pars interarticularis according to previously published studies (11, 15).

Tier 3, UTE MR protocol constituted of a single sagittal 3D Cones sequence. All protocol specifications are summarized in Table 1, no additional planning or reconstruction time was required for the sagittal 3D Cones sequence. The 3D Cones sequence uses a unique k-space sampling trajectory that samples data along cone surfaces in 3D (23). No post-processing of the UTE dataset was used for the readout. Axial UTE images were also obtained for illustration purposes in some cases, but they were not used for the readout. The used UTE sequences are prototype pulse sequences.

For the ancillary in vivo part of the study, lumbar MRI of human subjects comprised the same sequences used in Tier 1 and 3. No major changes to the protocol were needed, as the cadaveric study utilized MR sequences and coils that were readily translatable.

CT imaging

After the experimental fractures were surgically induced, the spine specimen were scanned using a 256-MDCT scanner (Revolution CT, GE Healthcare, Milwaukee, USA) with 120 kV and 100 mA and a slice thickness of 0.625 mm with a reconstruction diameter of 50 cm and a matrix of 512×512. The fracture gaps were measured on sagittal reformatted images perpendicular to the lower side of the fracture line using RadiAnt DICOM Viewer software (Medixant, Poznan, Poland) with a slice thickness of 0.625 mm by a radiologist (*initials - blinded for review*) who did not participate in the readout.

Detection of spondylolysis in images of cadaveric specimens

The assessment of spondylolysis detection of the vertebral segments between T12 and L5 was performed independently by two blinded, board-certified radiologists with fellowship training in musculoskeletal radiology. Reader 1 (R1) (*initials - blinded for review*) and reader 2 (R2) (*initials - blinded for review*) had 7 and 5 years of experience, respectively. The RadiAnt DICOM Viewer software (Medixant, Poznan, Poland) was used for assessment and provided the use of cross-reference lines and image leveling.

To reduce recall bias, we first waited 4 weeks after MRI before evaluating Tier 1 images, waited 2 weeks before reading Tier 2 images, and waited another 2 weeks before reading Tier 3 images, randomizing the order of samples between Tiers as well as readers. For this study, spondylolysis was detected as a continuous discontinuity in the cortical shell and cancellous bone in individual pars. For each Tier of images, the diagnostic confidence for the presence of spondylolysis was assessed using a 4-point scale: 1 (spondylolysis certainly absent), 2 (spondylolysis probably absent), 3 (spondylolysis probably present), 4 (spondylolysis certainly present), a scoring system used in previous studies by Lee et al. (24) and Jaeger et al. (25). For Tiers 1 and 2 where multiple sequences were evaluated, each reader noted which particular sequence was the most informative and decisive, if the reader found the pars to be positive for a fracture.

Statistics

Inter-reader agreement for the detection of spondylolysis of each individual pars interarticularis was calculated using linearly weighted Cohen's kappa (κ) analysis where coefficient of 0.21–0.40 indicated fair, 0.41–0.60 moderate, 0.61–0.80 good, and >0.81 indicated an excellent agreement (26). For subsequent analyses, in case of a disagreement, a consensus reading was performed and eventually the score from the senior reader was used.

For each Tier, the diagnostic performance (sensitivity, specificity, and receiver operatic characteristic area under the curve, AUC) and confidence (uncertain or wrong diagnosis) for the detection of spondylolysis was calculated using the surgical osteotomies as the reference standard. The sensitivity and specificity values were compared between Tiers, using McNemar's statistic separately for sensitivity in samples positive for pars defect, and for

specificity in samples negative for pars defect (27). AUC values were also compared (28) between Tiers. Diagnostic confidence values were also compared between Tiers using McNemar statistic. For statistical analysis, commercially available software was used (Systat 10, Systat Software, San Jose, CA). Statistical significance was set at a two-tailed p-value below 0.05.

RESULTS

Cadaveric Study

On the basis of the randomization, 20/46 (43%) pars interarticularis were selected for experimental fracture and 26/46 (57%) pars were selected to be left intact. The mean width of the experimental fracture gaps was 1.2 ± 0.3 mm (range 1.0 – 1.9 mm), only slightly wider than the thickness of the saw blade. Approximate reading time per specimen for each Tier was: Tier 1 = 4 min; Tier 2 = 3 min; Tier 3 = <1 min.

Using conventional sequences of Tier 1, the pars fractures were usually not visible on axial and sagittal T1 and T2 (Figures 1A) images, while the sagittal short tau inversion recovery (STIR) images often revealed the gap as a linear medium signal intensity (Figure 1B, arrow). In general, evaluation of pars fractures on axial images (Figure 2FG) was challenging due to varying oblique angles of the fractures to all three orthogonal planes, as well as a complex anatomy involving close proximity of pars to facet joints (Figure 2E) (29).

In Tier 2, by tilting the sagittal imaging plane or reformatting (Figure 2J, dashed line C), sagittal oblique spoiled gradient recall echo (SPGR) images (Figure 2C) revealed classic “Scottie Dog” sign that featured pars fracture at the neck of the dog (Figure 2C, arrow). Similarly, by tilting the axial imaging plane (Figure 2E, dashed line H) more orthogonal to the fracture, Tier 2 axial oblique STIR images (Figure 2H) also made it easier to detect the pars fractures. In Tiers 1 and 2, the sagittal STIR and the sagittal oblique SPGR, respectively, were the most decisive sequences.

Although the optimized sequences of Tier 2 were an improvement over conventional sagittal and axial sequences of Tier 1, Tier 3 UTE images allowed the most facile detection of pars fractures. All pars defects were as clearly and confidently visible on sagittal UTE images (Figures 1C and 2D, arrows) as they were on CT images (Figures 1D and 2D). The similarities between UTE and CT in image characteristics (albeit inverted) and the visibility of pars fractures due to the increased contrast between bone and fracture gap were striking. In a few difficult cases where the pars fractures were not visible on the conventional (Figure 3AB) and optimized conventional (Figure 3C) MR protocols, the single sagittal UTE sequence revealed the fractures with ease (Figure 3D, arrow).

Inter-reader agreement was good for conventional Tier 1 (κ=0.777; confidence interval, CI=0.647 to 0.907) and optimized Tier 2 (κ=0.847; CI=0.734 to 0.960), and excellent for CT or Tier 3 (κ=1.00; CI=1 to 1), suggesting an easier and straight-forward read for CT and Tier 3 UTE images compared to other Tiers.

Diagnostic performance (Table 2) was moderate for Tier 1 and 2, with a moderate sensitivity (0.70 to 0.75) and high (1.00) specificity. In contrast, CT and Tier 3 UTE MRI had both high sensitivity (1.00) and specificity (1.00). The Tier 3 sensitivity was statistically greater than Tier 1 sensitivity ($p=0.041$), and nearly significantly greater than Tier 2 sensitivity ($p=0.074$). There was no difference in specificity between the Tiers. Area under the ROC curve (Table 2) was also significantly greater for CT and Tier 3 (each area=1.00), compared to the areas for Tier 1 (0.89, $p=0.037$) or Tier 2 (0.873, $p=0.024$).

More importantly, the diagnostic confidence of Tier 3 was much greater than the other Tiers. Table 3 shows the percentage of uncertain but correct (i.e., spondylolysis probably absent or probably present, when a correct diagnosis is made) and wrong reads for each Tier. It can be seen that both Tiers 1 and 2 each have statistically higher (**, $p<0.001$) percentages of uncertain (>60 %) and wrong (>10%) diagnoses, compared to CT or Tier 3.

In Vivo Study

In two subjects with low back pain, Tier 1 sagittal conventional T2 (Figure 4AD) and Tier 3 UTE (Figure 4BE) MR images were obtained. The axial UTE (Figure 4CF) images were acquired for illustration purposes only and not used in the readout. In one subject, intact lumbar pars were well-depicted on the sagittal and axial UTE images (Figure 4BC). In the second subject, suffering from a progressive non-radicular low back pain, the UTE sequences accurately revealed spondylolysis (Figure 4EF, arrows) on L5 level of the male patient which was not visible on the conventional T2 image (Figure 4D) due to scar tissue within and near the pars defect. This subject had a wide, stage IV spondylolysis, according to Ralston et al. (22) with an early anterolisthesis.

DISCUSSION

Early diagnosis of spondylolysis is crucial in young individuals to increase the likelihood of non-surgical bone healing and to avoid nonunion with potential spondylolisthesis in bilateral cases (30, 31). In adults featuring almost exclusively long-standing terminal spondylolysis, diagnosis of spondylolysis is important to ascertain the cause of back pain and to aid planning of spinal fusion surgery as appropriate.

The UTE sequence used in our study was able to match diagnostic performance of the CT, while outperforming conventional and optimized conventional protocols significantly. On standard MR sequences, short T2 tissues such as cortical bone and osteofibrous scar tissue surrounding the pars defect unequivocally remain dark (32), while on UTE sequences these structures provide contrast. It should be noted that UTE technique is able to acquire MR signal from cortical bone (33), the MR signal from other soft tissues (including scar tissue) is markedly higher, leading to an appearance of dark bone surrounded by high signal intensity. These basic differences in MR signal characteristics provide the foundation for an improved detection of spondylolysis using UTE sequences. The sagittal UTE sequence is also practical in clinical routine requiring a scanning time of only 3 min and could therefore be added to a conventional MR protocol easily.

The sensitivity and specificity of our conventional and optimized lumbar MRI protocols for spondylolysis detection were similar those reported in previous studies. A recent meta-analysis published by Dhouib et al. (12) from 2017 included 1122 pars of young adults and children and showed a combined sensitivity of 81% (54 to 95% CI) and a combined specificity of 99% (98 to 100% CI) which is comparable to the results of our conventional (Tier 1) lumbar MR protocol. In studies that have investigated the diagnostic performance of a protocol similar to our optimized conventional (Tier 2) MR protocol, they showed a sensitivity of 86–92% and a specificity of 92–100% (10, 34). The slightly lower sensitivity of the optimized conventional MR protocol in our study could be explained by susceptibility artifacts introduced by small amounts of air and metal wear debris possibly introduced during sample preparation. Such artifacts were visible on a few SPGR images. Fortunately, UTE sequences are less prone to susceptibility artifacts of this kind (35, 36).

We have also demonstrated the feasibility of translating the UTE technique in vivo in a preliminary manner. In our human subjects with and without spondylolysis, image quality was similar to the specimen study, which was designed with clinical translation in mind. In future studies, the capacity of UTE technique to diagnose spondylolysis in adults and ultimately in the pediatric population should be further investigated. While the availability of our particular UTE sequence may not wide-spread, currently other sequences capable of ultrashort echo time can run on clinical MR systems from almost every major manufacturer (e.g., encoding time reduction with radial acquisition (PETRA) and zero echo time (ZTE) sequences) and have been increasingly used in medical imaging studies (37, 38). For example, the recently published study by Breighner et al. found great merit of ZTE sequences for bone imaging of the shoulder (39).

It should be clarified that our study does not address all stages of spondylolysis, including very early stages. According to Ralston et al. (22) there are four successive stages of spondylolysis. Our experimental fractures would fall between stage II “early spondylolysis” characterized by a hairline fracture and stage III “progressive spondylolysis” characterized by a wide pars defect. The other spondylolysis stages, prespondylolytic stage I “pars stress reaction” and stage IV “terminal spondylolysis” characterized by nonunion and sclerosis, could not be created experimentally, since these are dependent on edematous bone marrow response and bone remodeling in a living tissue. However, edematous bone marrow changes can be accurately detected using conventional fat-suppressed fluid-sensitive sequences (3, 15, 16, 22, 40), and it is likely that the diagnostic performance of all Tiers will be increased for even larger fractures of terminal stage spondylolysis (such as that seen in our subject in Figure 4EF, arrows). While our experimental fractures with ~1 mm width were fairly thin, it remains to be determined if even thinner hairline fractures could also be detected with UTE techniques.

Our study has further limitations. First, due to the small number of available specimens, we created an artificially large number of fractures (20 of 46 pars, at 2 or more levels in all specimens). This frequency exceeds the prevalence of about 5% in the adult population and about 50% in adolescent athletes with persistent back pain (3), usually occurring only at a single level at L5 (1). Second, our surgical preparation inherently constituted an artificial condition. However, we meticulously applied a technique previously published by Kepler et

al. (21), using even thinner oscillating saw blades of only 0.9 – 1 mm, while preserving the paravertebral soft tissue structures as good as possible. Nonetheless, the CT proved that the morphology and orientation of the experimental fractures were similar to natural fractures (41). Third, we did not include other types of MR sequences that may better visualize bone detail such as 3D Turbo spin echo MR imaging, susceptibility-weighted MR imaging (42) or "black bone" gradient echo MR imaging (43, 44). It would be useful to evaluate and compare the performance of these sequence for spondylolysis image. Fourth, to prevent air and fluid accumulation, the delicate fractures were filled with agarose gel. As described, we systematically identified the 8% agarose gel as the best candidate featuring MR signal characteristics similar to scar tissue that is frequently located within and in proximity to pars defects. Lastly, our study was performed at 3T only and therefore the results may or may not be transferable to lower field strength scanners. There are confounding issues such as susceptibility artifacts from cortical bone at 3T (45), that may vary with the field strength.

In conclusion, our study demonstrated that the detection of pars fractures using a single sagittal UTE MR sequence is superior in performance and confidence to conventional and optimized MR protocols at 3T, while matching those from CT evaluation. Furthermore, we demonstrated the feasibility of in vivo application of the UTE sequence in subjects with and without spondylolysis. We believe that UTE sequences offer a great potential for radiation-free bone imaging and will play an increasing role in patient care in the future.

REFERENCES

1. Jinkins JR, Matthes JC, Sener RN, Venkatappan S, Rauch R. Spondylolysis, spondylolisthesis, and associated nerve root entrapment in the lumbosacral spine: MR evaluation. AJR Am J Roentgenol. 1992;159(4):799–803. [PubMed: 1529846]
2. Hu SS, Tribus CB, Diab M, Ghanayem AJ. Spondylolisthesis and spondylolysis. Instr Course Lect. 2008;57:431–45. [PubMed: 18399601]
3. Micheli LJ, Wood R. Back pain in young athletes. Significant differences from adults in causes and patterns. Arch Pediatr Adolesc Med. 1995;149(1):15–8. [PubMed: 7827653]
4. Fredrickson BE, Baker D, McHolick WJ, Yuan HA, Lubicky JP. The natural history of spondylolysis and spondylolisthesis. The Journal of bone and joint surgery American volume. 1984;66(5):699–707. [PubMed: 6373773]
5. Bechtel W, Griffiths HJ, Eisenstadt R. The Pathogenesis of Spondylolysis. Investigative radiology. 1982;17(4):S29.
6. Pearce MS, Salotti JA, Little MP, et al. Radiation exposure from CT scans in childhood and subsequent risk of leukaemia and brain tumours: a retrospective cohort study. Lancet. 2012;380(9840):499–505. [PubMed: 22681860]
7. Beck NA, Miller R, Baldwin K, et al. Do oblique views add value in the diagnosis of spondylolysis in adolescents? The Journal of bone and joint surgery American volume. 2013;95(10):e65. [PubMed: 23677366]
8. Fadell MF, Gralla J, Bercha I, et al. CT outperforms radiographs at a comparable radiation dose in the assessment for spondylolysis. Pediatr Radiol. 2015;45(7):1026–30. [PubMed: 25712453]
9. Richards PJ, George J, Metelko M, Brown M. Spine computed tomography doses and cancer induction. Spine (Phila Pa 1976). 2010;35(4):430–3. [PubMed: 20081559]
10. Ganiyusufoglu AK, Onat L, Karatoprak O, Enercan M, Hamzaoglu A. Diagnostic accuracy of magnetic resonance imaging versus computed tomography in stress fractures of the lumbar spine. Clin Radiol. 2010;65(11):902–7. [PubMed: 20933645]

11. Campbell RS, Grainger AJ, Hide IG, Papastefanou S, Greenough CG. Juvenile spondylolysis: a comparative analysis of CT, SPECT and MRI. Skeletal radiology. 2005;34(2):63–73. [PubMed: 15668821]
12. Dhouib A, Tabard-Fougere A, Hanquinet S, Dayer R. Diagnostic accuracy of MR imaging for direct visualization of lumbar pars defect in children and young adults: a systematic review and meta-analysis. Eur Spine J. 2017.
13. Yamaguchi KT, Jr., Skaggs DL, Acevedo DC, Myung KS, Choi P, Andras L. Spondylolysis is frequently missed by MRI in adolescents with back pain. J Child Orthop 2012;6(3):237–40. [PubMed: 23814624]
14. Johnson DW, Farnum GN, Latchaw RE, Erba SM. MR imaging of the pars interarticularis. AJR Am J Roentgenol. 1989;152(2):327–32. [PubMed: 2783509]
15. Dunn AJ, Campbell RS, Mayor PE, Rees D. Radiological findings and healing patterns of incomplete stress fractures of the pars interarticularis. Skeletal radiology. 2008;37(5):443–50. [PubMed: 18283450]
16. Rush JK, Astur N, Scott S, Kelly DM, Sawyer JR, Warner WC, Jr.. Use of magnetic resonance imaging in the evaluation of spondylolysis. J Pediatr Orthop. 2015;35(3):271–5. [PubMed: 24978120]
17. Williams A, Qian Y, Golla S, Chu CR. UTE-T2 * mapping detects sub-clinical meniscus injury after anterior cruciate ligament tear. Osteoarthritis Cartilage. 2012;20(6):486–94. [PubMed: 22306000]
18. Springer F, Steidle G, Martirosian P, Syha R, Claussen CD, Schick F. Rapid assessment of longitudinal relaxation time in materials and tissues with extremely fast signal decay using UTE sequences and the variable flip angle method. Investigative radiology. 2011;46(10):610–7. [PubMed: 21577126]
19. Siriwanarangsun P, Statum S, Biswas R, Bae WC, Chung CB. Ultrashort time to echo magnetic resonance techniques for the musculoskeletal system. Quant Imaging Med Surg. 2016;6(6):731–43. [PubMed: 28090449]
20. Han M, Larson PE, Liu J, Krug R. Depiction of achilles tendon microstructure in vivo using high-resolution 3-dimensional ultrashort echo-time magnetic resonance imaging at 7 T. Investigative radiology. 2014;49(5):339–45. [PubMed: 24500089]
21. Kepler CK, Pavlov H, Herzog RJ, Rawlins BA, Endo Y, Green DW. Comparison of a fluoroscopic 3-dimensional imaging system and conventional CT in detection of pars fractures in the cadaveric lumbar spine. J Spinal Disord Tech. 2012;25(8):429–32. [PubMed: 22143044]
22. Ralston S, Weir M. Suspecting lumbar spondylolysis in adolescent low back pain. Clin Pediatr (Phila). 1998;37(5):287–93. [PubMed: 9597294]
23. Gurney PT, Hargreaves BA, Nishimura DG. Design and analysis of a practical 3D cones trajectory. Magn Reson Med. 2006;55(3):575–82. [PubMed: 16450366]
24. Lee MJ, Kim MJ, Yoon CS, Chung YE, Han SJ, Koh H. Gadopentetate dimeglumine-enhanced MR cholangiopancreatography in infants with cholestasis. Pediatr Radiol. 2011;41(4):488–94.
25. Jager HR, Mansmann U, Hausmann O, Partzsch U, Moseley IF, Taylor WJ. MRA versus digital subtraction angiography in acute subarachnoid haemorrhage: a blinded multireader study of prospectively recruited patients. Neuroradiology. 2000;42(5):313–26. [PubMed: 10872150]
26. Landis JR, Koch GG. The measurement of observer agreement for categorical data. Biometrics. 1977;33(1):159–74. [PubMed: 843571]
27. Newcombe RG. Simultaneous comparison of sensitivity and specificity of two tests in the paired design: a straightforward graphical approach. Stat Med. 2001;20(6):907–15. [PubMed: 11252012]
28. Hanley JA, McNeil BJ. The meaning and use of the area under a receiver operating characteristic (ROC) curve. Radiology. 1982;143(1):29–36. [PubMed: 7063747]
29. Dougherty SP, Jahnke RW, Sibbitt RR. THE PSEUDOFACET SIGN – CT AND MR DIAGNOSIS OF SPONDYLOLYSIS. Investigative radiology. 1989;24(12):S121.
30. Morita T, Ikata T, Katoh S, Miyake R. Lumbar spondylolysis in children and adolescents. J Bone Joint Surg Br. 1995;77(4):620–5. [PubMed: 7615609]
31. McCleary MD, Congeni JA. Current concepts in the diagnosis and treatment of spondylolysis in young athletes. Curr Sports Med Rep. 2007;6(1):62–6. [PubMed: 17212915]

32. Sotiropoulos S, Chafetz NI, Lang P, et al. Differentiation between postoperative scar and recurrent disk herniation: prospective comparison of MR, CT, and contrast-enhanced CT. AJNR Am J Neuroradiol. 1989;10(3):639–43. [PubMed: 2501998]
33. Du J, Carl M, Bydder M, Takahashi A, Chung CB, Bydder GM. Qualitative and quantitative ultrashort echo time (UTE) imaging of cortical bone. J Magn Reson. 2010;207(2):304–11. [PubMed: 20980179]
34. Ang EC, Robertson AF, Malara FA, et al. Diagnostic accuracy of 3-T magnetic resonance imaging with 3D T1 VIBE versus computer tomography in pars stress fracture of the lumbar spine. Skeletal radiology. 2016;45(11):1533–40. [PubMed: 27614965]
35. Chang EY, Bae WC, Chung CB. Imaging the knee in the setting of metal hardware. Magn Reson Imaging Clin N Am. 2014;22(4):765–86. [PubMed: 25442032]
36. Kumar NM, de Cesar Netto C, Schon LC, Fritz J. Metal Artifact Reduction Magnetic Resonance Imaging Around Arthroplasty Implants: The Negative Effect of Long Echo Trains on the Implant-Related Artifact. Investigative radiology. 2017;52(5):310–6. [PubMed: 28079703]
37. Chang EY, Du J, Chung CB. UTE imaging in the musculoskeletal system. J Magn Reson Imaging. 2015;41(4):870–83. [PubMed: 25045018]
38. Grodzki DM, Jakob PM, Heismann B. Ultrashort echo time imaging using pointwise encoding time reduction with radial acquisition (PETRA). Magn Reson Med. 2012;67(2):510–8. [PubMed: 21721039]
39. Breighner RE, Endo Y, Konin GP, Gulotta LV, Koff MF, Potter HG. Technical Developments: Zero Echo Time Imaging of the Shoulder: Enhanced Osseous Detail by Using MR Imaging. Radiology. 2018;286(3):960–6. [PubMed: 29117482]
40. Hollenberg GM, Beattie PF, Meyers SP, Weinberg EP, Adams MJ. Stress reactions of the lumbar pars interarticularis: the development of a new MRI classification system. Spine (Phila Pa 1976). 2002;27(2):181–6. [PubMed: 11805665]
41. Saifuddin A, White J, Tucker S, Taylor BA. Orientation of lumbar pars defects: implications for radiological detection and surgical management. J Bone Joint Surg Br. 1998;80(2):208–11. [PubMed: 9546445]
42. Bender YY, Diederichs G, Walter TC, et al. Differentiation of Osteophytes and Disc Herniations in Spinal Radiculopathy Using Susceptibility-Weighted Magnetic Resonance Imaging. Investigative radiology. 2017;52(2):75–80. [PubMed: 27548342]
43. Eley KA, Watt-Smith SR, Golding SJ. "Black Bone" MRI: a potential non-ionizing method for three-dimensional cephalometric analysis--a preliminary feasibility study. Dento maxillo facial radiology. 2013;42(10):20130236. [PubMed: 24052254]
44. Robinson AJ, Blaser S, Vladimirov A, Drossman D, Chitayat D, Ryan G. Foetal "black bone" MRI: utility in assessment of the foetal spine. The British journal of radiology. 2015;88(1046): 20140496. [PubMed: 25496509]
45. Bradley WG, Jr., Pros and cons of 3 tesla MRI. J Am Coll Radiol. 2008;5(8):871–8. [PubMed: 18657781]

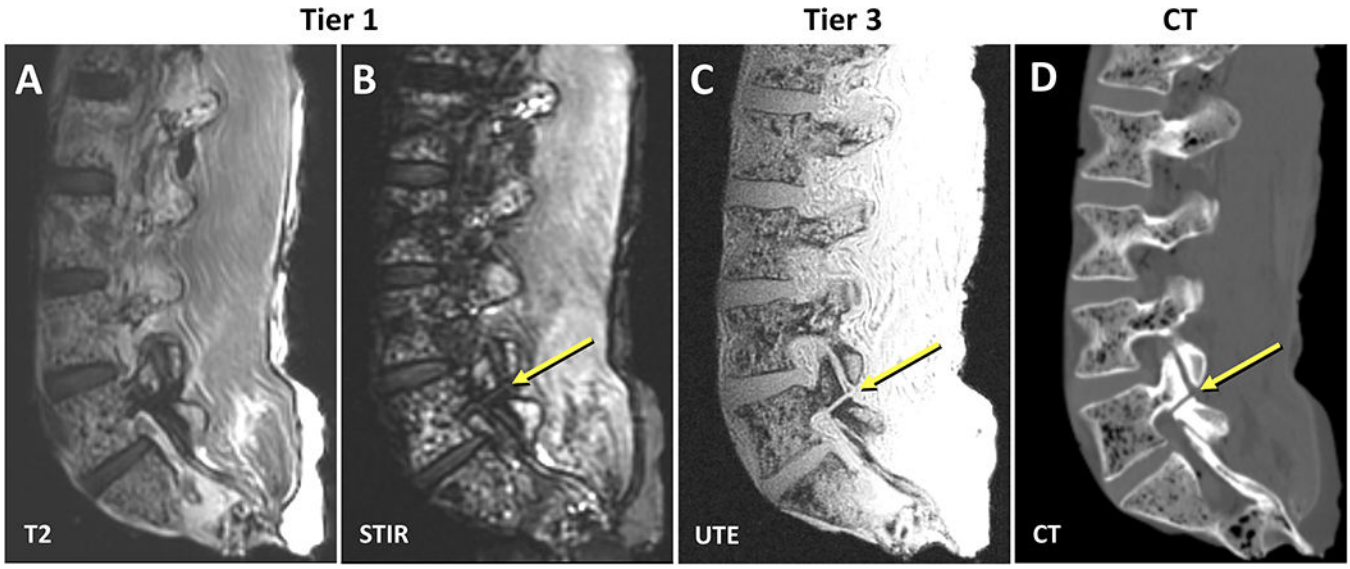

Figure 1.

Right-sided imaging of cadaveric spine from a 42-year-old female donor, showing typical sagittal images of an experimental pars fracture at L5. On the conventional T2 images (**A**) the experimental pars defect on the right L5 level is not visible. The STIR sequence (**B**) shows the pars defect to some extent (arrow). In contrast, both the UTE (**C**) and the CT (**D**) images clearly depict the very thin experimental pars fracture, ~1 mm in width.

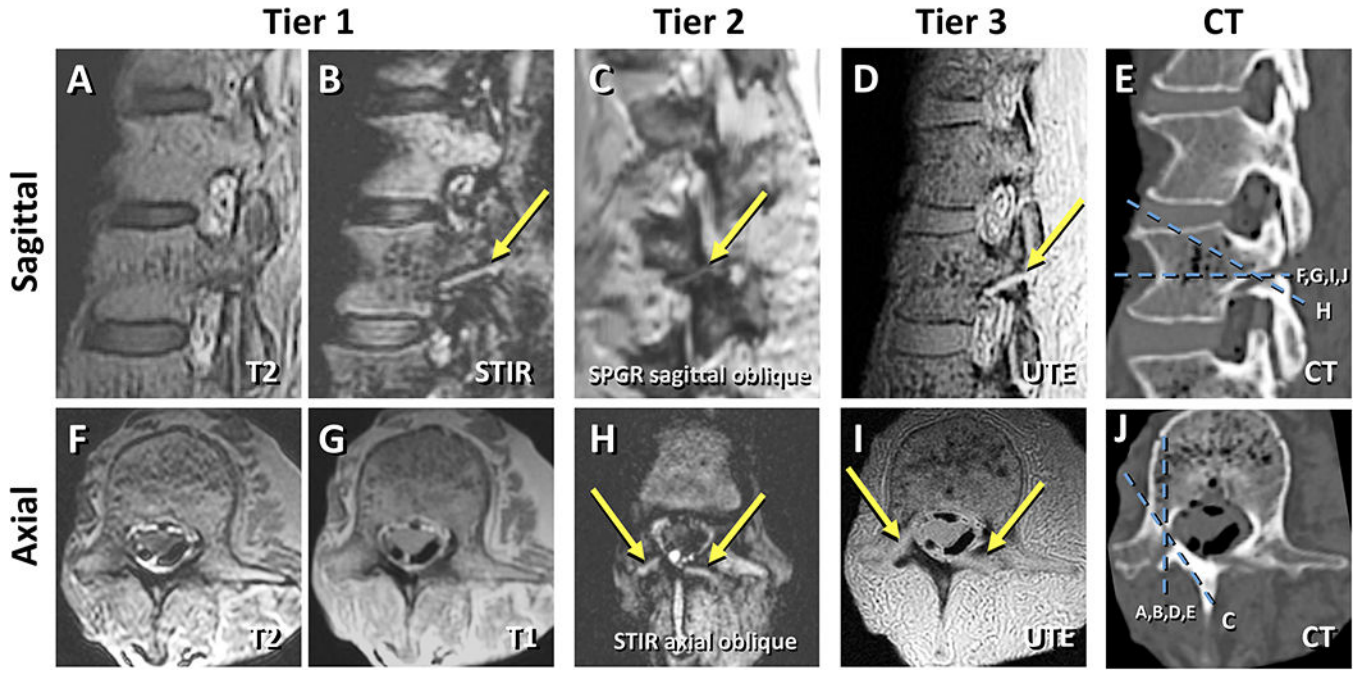

Figure 2.

Imaging of cadaveric spine from a 56-year-old female, showing representative images from all Tiers. Tier 1 (**A, B, F, G**), Tier 2 (**C, H**), Tier 3 (**D**), and CT (**E, J**) images are shown. Among the Tier 1 images, pars defect created on L1 level was not visible on sagittal T1 (not shown), sagittal T2 (**A**), axial T2 (**F**), and axial T1 (**G**) images, but it was moderately visible on sagittal STIR image (**B**, arrow). The rather horizontal orientation of the pars fracture, in combination with a slice thickness of 3.5 mm for the axial T2 (**F**) and T1 (**G**) sequences, hampered the detection of pars defects considerably. Among the Tier 2 images, sagittal oblique SPGR revealed the fracture at the neck of the "Scotty Dog" sign (**C**, arrow), and axial oblique STIR revealed the bilateral fractures with reduced partial volume artifact (**H**, arrows). Axial oblique T1 images (not shown) were less effective at revealing the fractures due to low signal intensity at the gap. In comparison, sagittal UTE (**D**) and CT (**E**) images clearly depicted the pars fracture (arrow) as a linear discontinuity. The pars fractures are also clearly visible in axial UTE (**I**, arrows) and CT (**J**) images but the margins of the defect are soft due to the partial volume artifact. These axial UTE and CT images were acquired for illustration purposes only and not used in the readout. The reference lines for the respective imaging planes are shown in the CT images (**E, J**).

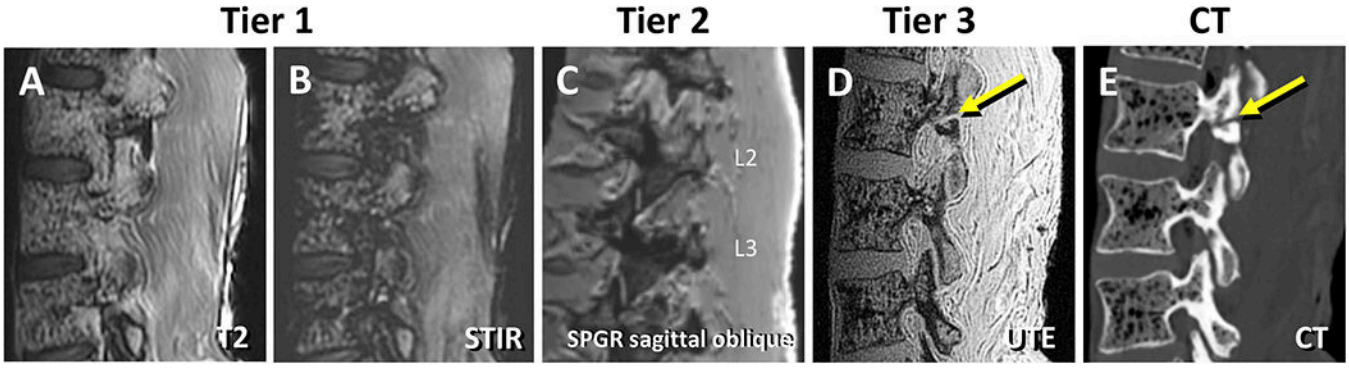

Figure 3.

Imaging of cadaveric spine from a 42-year-old female, showing a difficult case where the pars fractures were not detected on Tier 1 and 2 images. On the conventional sagittal T2 (**A**) and STIR (**B**) images (Tier 1), as well as on the sagittal oblique SPGR (**C**) images (Tier 2), the right-sided pars fracture at the L2 level was not detected during the readout. In contrast, on the sagittal UTE (**D**) and CT (**E**) images, a thin fracture (arrows) was easily detected with high diagnostic confidence.

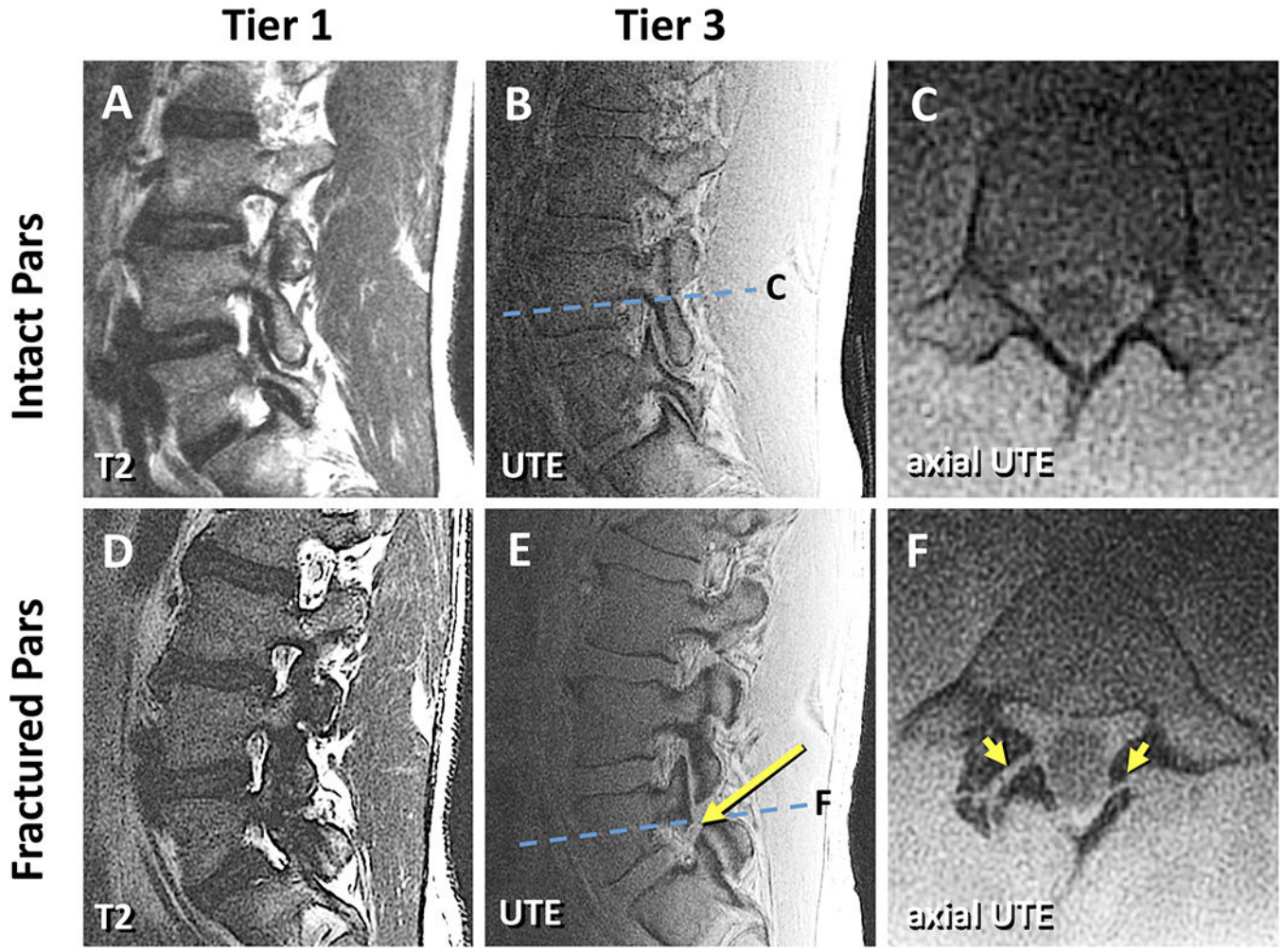

Figure 4.

In vivo imaging of subjects without (**A, B, C**) and with (**D, E, F**) spondylolysis. In a 46-year-old male subject (**A-C**) the right-sided L4 pars was intact on the sagittal T2 (**A**) as well as on the sagittal UTE (**B**) and axial UTE (**C**) image. In images of a 45-year-old male subject with bilateral terminal spondylolysis at L5 (**D-F**), sagittal T2 image (**D**) could not depict the fracture. In comparison, the corresponding sagittal (**E**) and axial (**F**) UTE images clearly depicted the pars defects (arrows), indicating the feasibility of in vivo application of the UTE sequence in subjects with and without spondylolysis.

Table 1.

MR sequence parameters of Tier 1–3.

For the axial oblique sequences of Tier 2, the axial imaging plane was sloping down towards rear (Figure 2E, dashed line H) since the pars is oriented obliquely to all three orthogonal planes. An oblique sagittal multiplanar reconstruction for the right and the left side was performed for the SPGR sequence.

	Sequence	TR (msec)	TE (msec)	Reconstruction Matrix	Slice (mm)	FOV (cm)	BW (±)	FA (°)	Voxel dimension (xyz, mm)	Scan time (min)
Tier 1	Sagittal SE T1	2297	24	256×256	3	24	62.5	90	0.94×0.94×3	2:34
	Sagittal SE T2	4618	102	256×256	3	24	62.5	90	0.94×0.94×3	2:14
	Axial SE T1	774	13	256×256	3.5	16	62.5	90	0.63×0.63×3.5	2:59
	Axial SE T2	9733	102	256×256	3.5	16	62.5	90	0.63×0.63×3.5	2:07
	Sagittal STIR	6466	60	256×256	3	24	31.25	90	0.94×0.94×3	3:07
Tier 2	Axial oblique SE T1	2297	24	256×256	3	24	62.5	90	0.94×0.94×3	2:34
	Axial oblique STIR	14938	60	256×256	3.5	16	31.25	90	0.63×0.63×3.5	3:38
	Sagittal SPGR	27	7	256×256	2	24	20.8	30	0.94×0.94×2	6:43
Tier 3	Sagittal 3D Cones	44.3	0.05	256×256	2	24	125	2	0.94×0.94×2	3:12

Abbreviations: SE = Spin echo; STIR = short tau inversion recovery; SPGR = spoiled gradient recall echo; 3D Cones = name of a particular UTE sequence; TR = time to repetition; TE = time to echo; FOV = field of view; BW = bandwidth; FA = flip angle; xy = in-plane; z= through-plane.

Table 2.

Diagnostic performance.

Summary of the diagnostic performance of each MR Tier and CT images for pars fracture detection using the surgical osteotomies as the reference standard. The sensitivity was moderate (0.70 to 0.75) for Tier 1 and 2. In contrast, CT and Tier 3 MR had higher sensitivity values (1.00). The Tier 3 sensitivity was statistically higher than Tier 1 sensitivity ($p<0.05$, *), and nearly significantly higher than Tier 2 sensitivity ($p=0.074$, †). There was no difference in the specificity values between the imaging modalities. The area under the receiver operating characteristic (ROC) curve was statistically greater for CT and Tier 3 compared to Tiers 1 and 2 (each $p<0.05$, *).

	Tier 1: Conventional				Tier 2: Optimized				CT or Tier 3: UTE			
Pars Fracture	**Present**		**Absent**		**Present**		**Absent**		**Present**		**Absent**	
	Certainly	**Probably**	**Probably**	**Certainly**	**Certainly**	**Probably**	**Probably**	**Certainly**	**Certainly**	**Probably**	**Probably**	**Certainly**
Present (n=20)	5	9	6	0	3	12	3	2	20	0	0	0
Absent (n=26)	0	0	19	7	0	0	16	10	0	0	0	26
Sensitivity	0.70 *				0.75 †				1.00			
Specificity	1.00				1.00				1.00			
ROC Area Under the Curve	0.89 *				0.87 *				1.00			

Table 3.

Diagnostic confidence.

Diagnostic confidence of imaging modalities expressed as the percentage of uncertain but correct reads (i.e., spondylolysis probably absent or probably present, when a correct diagnosis is made) and wrong diagnoses. Results are divided according to the surgical osteotomy reference standard into “present” (pars fracture is present), “absent” (pars fracture is absent) and all cases. Notably, Tiers 1 and 2 have statistically higher ($p<0.001$, **) percentages of uncertain (>60 %) and wrong (>10%) diagnoses, compared to CT or Tier 3.

	Tier 1		Tier 2		CT or Tier 3	
Pars Fracture	**Uncertain**	**Wrong**	**Uncertain**	**Wrong**	**Uncertain**	**Wrong**
All cases (n=46)	61% **	13% **	61% **	11% **	0%	0%